Mon. Not. R. Astron. Soc. **297,** 990–998 (1998)

Are AGN broad emission lines formed by discrete clouds? Analysis of Keck high-resolution spectroscopy of NGC 4151

Nahum Arav,[1]★† Tom A. Barlow,[2] Ari Laor,[3] Wallace L. W. Sargent[2] and Roger D. Blandford[1]

[1]*Theoretical Astrophysics, Caltech 130-33, Pasadena, CA 91125, USA*
[2]*Department of Astronomy, Caltech 105-24, Pasadena, CA 91125, USA*
[3]*Physics Department, Technion, Haifa 3200, Israel*

Accepted 1998 January 5. Received 1997 December 15; in original form 1997 July 15

ABSTRACT

We search for a direct signature of discrete 'clouds' in the broad-line region (BLR) of the Seyfert galaxy NGC 4151. For this purpose we apply cross-correlation (CC) analysis to a high-resolution Keck spectrum of the galaxy. No such signature is found in the data. In order for cloud models to be compatible with this result, there must be at least $\sim 3\times10^7$ emitting clouds in the BLR, where the limit is based on simulation of a homogeneous cloud population. More realistic distributions increase the lower limit to above 10^8. These numbers are an order-of-magnitude improvement on our previous limit from Mrk 335, where the improvement comes from higher signal-to-noise ratio (S/N), broader lines and refined simulations. Combined with the predicted upper limit for the number of emitting clouds in NGC 4151 (10^6–10^7), the derived lower limit puts a strong constraint on the cloud scenario in the BLR of this object. Similar constraints can be placed on models where the emission originates in streams and sheets. Thus, this investigation suggests that the broad emission lines (BELs) in NGC 4151, and by extension in all AGNs, are not made of an ensemble of discrete independent emitters.

Key words: galaxies: active – galaxies: individual: NGC 4151 – quasars: emission lines – galaxies: Seyfert.

1 INTRODUCTION

Broad emission lines (BELs) are among the most prominent feature observed in active galactic nuclei (AGN). The standard picture is that the BEL material is in the form of dense clouds with a volume filling factor of $\sim10^{-6}$, illuminated by a central ionizing continuum source (Netzer 1990; Arav et al. 1997). Two main cloud models appear in the literature. One is the two-phase model in which cool clouds ($T\sim10^4$ K) are embedDed in a hot medium with $T\sim10^8$ K which confines the clouds (Krolik, McKee & Tarter 1981). Another class of models creates the BELs out of stellar atmospheres or 'bloated' stars (Scoville & Norman 1988; Kazanas 1989; Alexander & Netzer 1994). In these models the individual sources are slow (~10 km s^{-1}) outflows emanating from supergiant stars. For further description of the two-phase and bloated star models, including some of their shortcomings, see Arav et al. (1997) and references therein. Alternatives to the cloud picture can be found in magnetic-driven winds (Emmering, Blandford & Shlosman 1992), and in models of disc emission coupled with winds (Chiang & Murray 1996).

In a previous paper (Arav et al. 1997) we described an investigation aimed at testing the cloud picture. Here we give a brief description of the basic idea and our methodology. An ensemble of discrete emitting units is expected to give a smooth line profile only when the number of units approaches infinity. For any finite number of randomly distributed clouds there will be fluctuations assocaited with the discreteness of the profile-building blocks. The same microstructure that is caused by the fluctuations in one line profile should appear in different observations of the same line, and in different lines that arise from the same ion. On the other hand photon shot noise, which is a major cause of fluctuations [in essence the signal-to-noise ratio (S/N) of the observation], is a random process, and therefore there is

★E-mail: arav@tapir.caltech.edu
†Present address: IGPP, Lawrence Livermore Nat. Laboratory, L-413, PO Box 808, Livermore, CA 94550, USA.

hope of obtaining a clear distinction between the two sources of fluctuation. Furthermore, because fluctuations caused by clouds in two different profiles ought to correlate along the entire profile, we should be able to detect fluctuations even if they are locally smaller than the random photon shot noise.

The most straightforward way to test for similar microstructure in different profiles is to use cross-correlation (CC) techniques (for details see Arav et al. 1997). Such an approach was used by Atwood, Baldwin & Carswell (1982) on moderate-resolution spectra of Mrk 509, and the lack of a strong CC at zero velocity shift in their data was interpreted as a lower limit of 5×10^4 for the number of emitting clouds (N_c). By using an improved CC analysis on high-quality data from Mrk 335, and extensive Monte Carlo simulations, we were able to put a lower limit of $N_c \gtrsim 3\times10^6$ for this object. This limit applies to identical clouds with realistic temperature ($T=2\times10^4$ K) and optical depth ($\sim10^4$ in the Hα line). As the lower limit on N_c is at least 30 times larger than the maximum number of stars in the bloated star models, these models can be ruled out, unless the line width of the gas associated with an individual star exceeds the unrealistically large value of 100 km s^{-1}. Simple photoionization arguments yield estimates for the largest possible number of individual clouds without adhering to a specific cloud model. Therefore, it is of great interest to try to constrain this model-independent estimate. In Mrk 335 the photoionization estimate for the upper limit of N_c varies between 10^7 and 10^8 with large uncertainties, and thus is compatible with our lower limit. A significant improvement in the limit on N_c is needed in order to confront the photoionization estimate.

To achieve this goal we observed NGC 4151 and analysed its BELs. For our purposes, this object has three advantages compared with Mrk 335.

(i) Reverberation studies (Maoz et al. 1991; see also a more recent campaign: Crenshaw et al. 1996; Edelson et al. 1996; Kaspi et al. 1996) indicate a BLR size of roughly 9 light-days. Substituting this number into our estimate of N_c (Arav et al. 1997), we obtain an upper limit of 10^7clouds (or 10^6 using the estimate found in Netzer 1990) in NGC 4151, which is an order of magnitude *smaller* than that in Mrk 335. These estimates are $\propto U^{-4}$, where U is the ionization parameter, and the above upper limits are for the commonly used value of $U=0.1$.

(ii) In spite of being less luminous, the closer distance of NGC 4151 makes it roughly 2 mag brighter than Mrk 335. The resultant higher S/N increases the Monte-Carlo-derived lower limit for N_c.

(iii) The BELs in NGC 4151 are three times wider than in Mrk 335. With all else equal, three times more clouds are needed to cover a three times wider line.

Advantages (ii) and (iii), combined with improvements in our algorithms, increase the lower limit on N_c to 3×10^7, an order of magnitude *larger* than that for Mrk 335. As the photoionization estimate for the upper limit on N_c is an order of magnitude lower, the combined effect is an improvement of two orders of magnitude in the constraint of this model-independent estimate.

A possible caveat comes from the fact that we used clouds with a number density of $\simeq10^{10}$ cm^{-2} in our upper limit estimates on N_c. This n_H is assumed because the C III] λ1909 BEL is strongly quenched at higher densities. However, models where a significant fraction of the Balmer line emission comes from a higher density gas were proposed in the literature (Ferland & Rees 1988). The upper limit on N_c for these models will be substantially higher. In order to test these models, a similar experiment to the one we show here should be performed on the C iii] λ1909 BEL in NGC 4151, for which the upper limit estimates on N_c should hold for all moels. This will require high-resolution spectroscopy with the *HST*.

In this paper we describe the NGC 4151 observations (Section 2), present the results of the CC analysis (Section 3), describe our Monte Carlo simulations from which we obtain the lower limits on N_c for different emission entities (Section 4) and discuss the implications of these results (Section 5).

2 DATA ACQUISITION AND REDUCTION

The HIRES spectra for the Seyfert galaxy NGC 4151 were obtained with the Keck I telescope on 1996 May 22. We acquired four exposures totalling 56 minutes. For the purpose of our analysis two exposures suffice, but by acquiring four we reduce the systematic errors in the data. Each exposure used a 0.86-arcsec slit (3 pixels) for a resolution of approximately 6.3 km s^{-1}. The actual resolution varies from about 6.0 to 6.5 km s^{-1} FWHM because of the change in dispersion across each 4200 km s^{-1} wide echelle order. The wavelength coverage was 4400 to 6800 Å with some gaps beyond 5000 Å. The S/N per (3-pixel) resolution element in the total exposure ranged from about 300 in the continuum up to $\sim$800 and $\sim$400 for the peak of the BEL components of the Hα and Hβ lines, respectively. The wavelength calibration error is about 0.1 pixel (0.2 km s^{-1}) rms and rises to a maximum error of about 0.3 pixel (0.6 km s^{-1}). This is the relative error across the spectrum. The absolute wavelength error is about 0.3 pixel (0.6 km s^{-1}), so altogether there can be up to $\sim$1 km s^{-1} error in the absolute wavelength value at any given pixel.

Severe fluxing errors occur when trying to combine echelle orders into a single continuous spectrum. This problem was exacerbated by the narrow-line-region emission, which has an angular extent larger than the 1-arcsec FWHM of the continuum spatial profile. As a result, the shapes of structures larger than about 20 Å are strongly affected by the rescaling process necessary to average the exposures. Relative flux level errors of 5–20 per cent may occur across sections of spectrum larger than 20 Å. The data was reduced using our own reduction package (Barlow & Sargent 1997), which automatically traces the orders and ignores anomalous radiation events in the sky region. As the narrow-emission-line region is resolved, we could not use profile modelling to correct for cosmic rays in the object. The cosmic rays were corrected after extracting the spectra and are evident as 'spikes' in the error spectrum. Fig. 1 shows the observed Hα and Hβ line profiles.

3 CROSS-CORRELATION ANALYSIS

For the CC analysis we used the same algorithm as used in Arav et al. (1997). First we fitted the same velocity segment

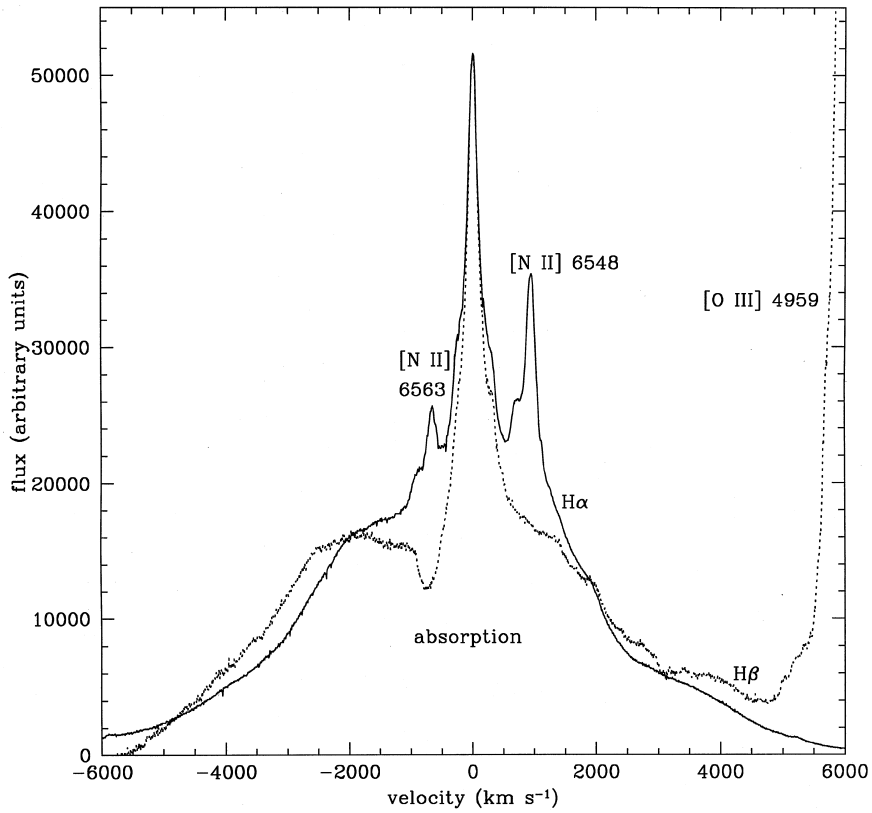

Figure 1. Observed profiles of the Hα (solid line) and Hβ (dotted line) lines in NGC 4151 (continuum-subtracted), in an arbitrary scaling that matches the peaks of the narrow-line components. Some associated feature are also labelled.

of two line profiles with eighth-order polynomials. Fig. 2 shows the two Hα data segments and fits that are used for calculating the CC function shown in Fig. 3. Each data segment is composed of two different exposures and the segments are labelled A (Fig. 2 top) and B (Fig. 2 bottom) in Figs 4 and 5. The reduced χ^2 for the fits were 1.01 (A) and 0.98 (B). This assures that systematic residuals are small (otherwise χ^2 would be significantly larger than 1), and that the fit is not too good (χ^2 significantly less than 1). As the given errors are caused purely by photon counting statistics, the reduced $\chi^2 \simeq 1$ result guarantees that on small scales the errors are governed by photon shot noise. A close look at the data in Fig. 2, in which the scale is magnified by a factor of 3 compared with Fig. 1, shows the similarities and differences between two separate observations of Hα (each is made up of two exposures). The profiles were first normalized to approximately the same flux level and then shifted by a small constant flux for ease of comparison. Over most of the velocity interval the ratio of the profile deviates by less than 1 per cent. However, in the interval between 2600 and 3200 km s^{-1} the ratio changes by up to 5 per cent as a result of the problems discussed in Section 2. These fluctuations occur on scales $\gtrsim$200 km s^{-1}, and thus do not significantly affect the search for a CC detection on scales of a few tens of km s^{-1}.

Following the definition in Arav et al. (1997), we calculated the CC function of the residuals extracted from Fig. 2. The result is shown in Fig. 3. We used only the red wing of Hα because the blue wing contains numerous atmospheric absorption lines which give rise to a strong CC($\Delta v = 0$) value, which is, of course, unrelated to the signature we hope to find. We also did not use the velocity interval 0–1600 km s^{-1}, because it is dominated by the narrow Hα and N II emission lines. Two more CC functions are shown in Fig. 4: the CC function for the red wing of Hβ (the blue wing gave a similar result) and the CC function of the composite observation of Hα and Hβ in a specific velocity interval. As in the case of Mrk 335, there is no significant CC at zero velocity shift. In order to try to detect a possible CC on larger scales approprite to realistic clouds (Arav et al. 1997), we tried Gaussian smoothing the CC function with velocity widths of up to 50 km s^{-1}. No significant CC was detected on these scales either (as expected by eye inspection of Figs 3 and 4).

4 MONTE CARLO SIMULATIONS

The lack of a CC signature in the data has implications for our understanding of the character and disposition of the line-emitting gas. We consider this problem in some generality by assuming, in turn, that the gas is organized in fundamental units of increasing dimensionality and that these elements are distributed in velocity space in an essentially uncorrelated manner.

4.1 Clouds

This is effectively the zero-dimensional case and is a feature of most published models (e.g. Krolik et al. 1981; Netzer 1990). We suppose that the gas is localized, in the form of

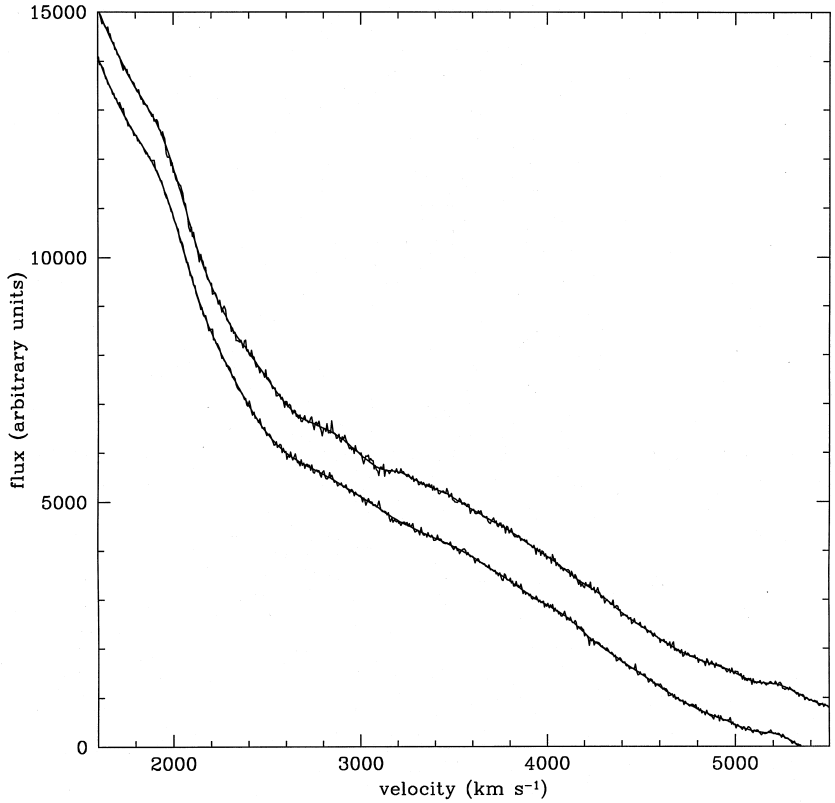

Figure 2. Two different data segments of Hα that were used to calculate the CC function shown in Fig. 3. The smooth lines that thread the data are the polynomial fits for these segments.

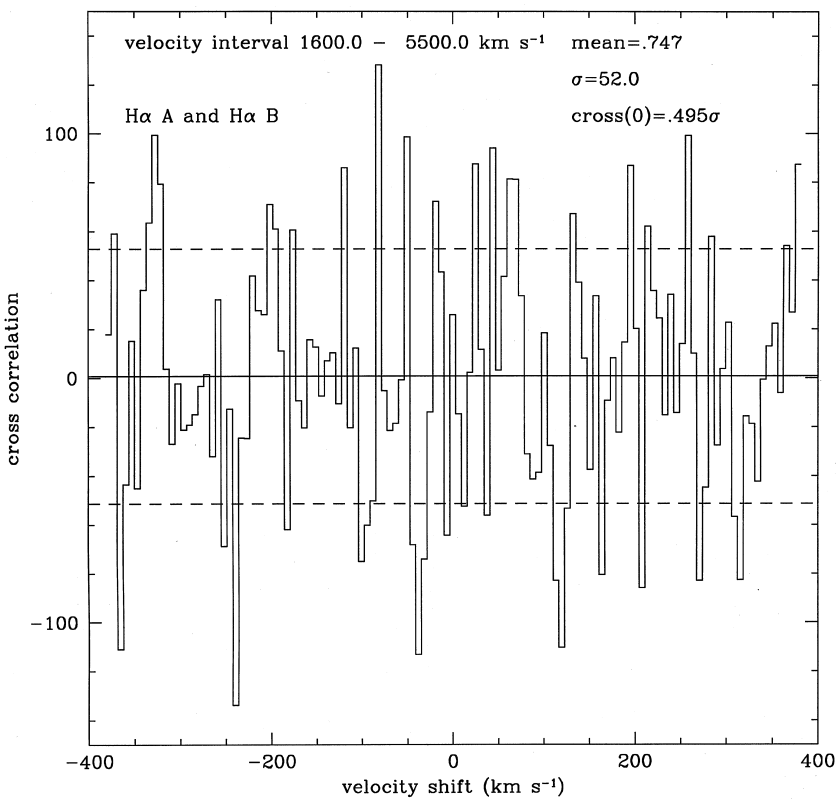

Figure 3. Cross-correlation (CC) function of the residuals (data − fit) for the data segments shown in Fig. 2. The CC units are arbitrary. No significant CC value is evident at zero velocity shift which would have been the signature of emission from discrete units. The histogram is the CC function, the dashed lines are $\pm 1\sigma$, cross(0) is the value of the function at zero velocity shift in σ units and the solid line is the mean of the function.

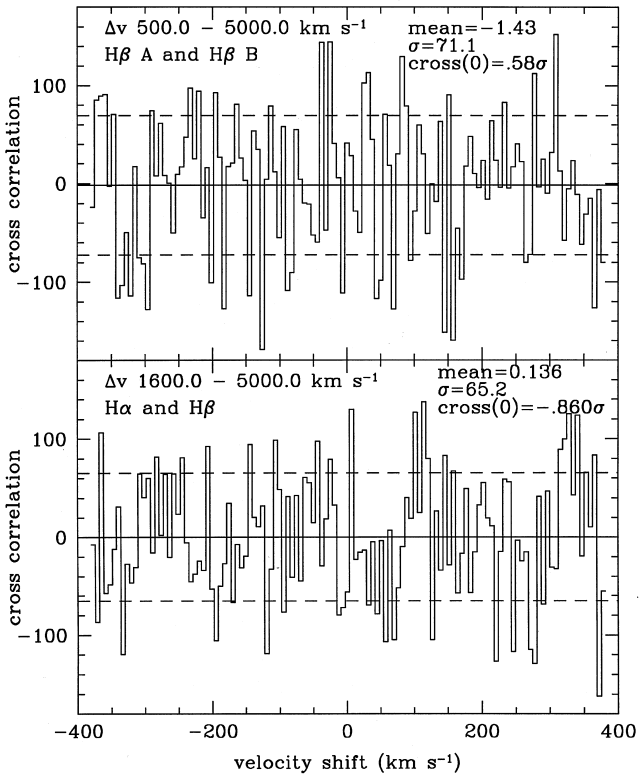

Figure 4. Cross-correlation function for Hβ A and Hβ B (upper panel), and for the complete data of Hα and Hβ (lower panel), similar to Fig. 3. Again no significant CC is seen at zero velocity shift.

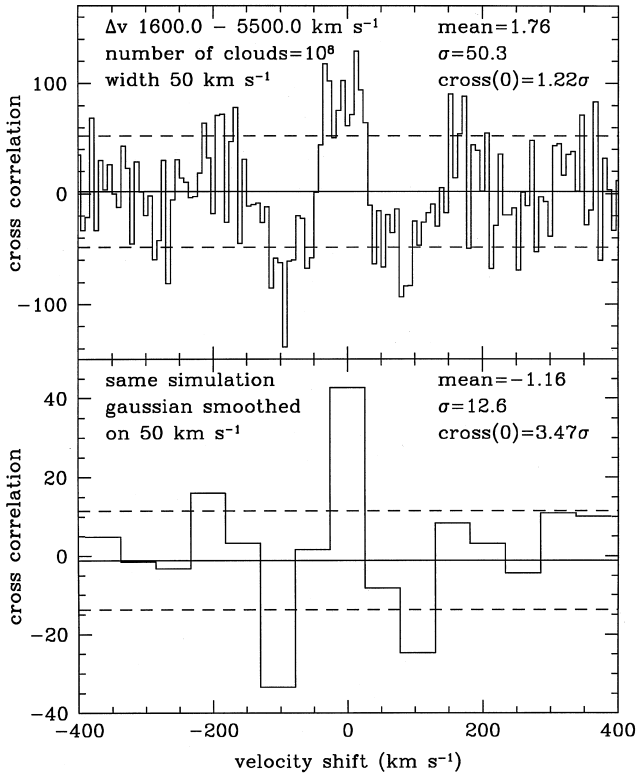

Figure 5. Top panel: CC function for simulated Hα profiles in a presentation similar to Fig. 3. The line profile is made from a distribution of 10^8 clouds where $dN_c/dL \propto L^{-1}$ (see text). Bottom panel: the same simulation where the CC was smoothed on a scale corresponding to the width of the clouds. The significant CC($\Delta v = 0$) from this cloud distribution is evident.

individual clouds characterized by a velocity width δv at least as large as the ion thermal speeds at a temperature $\sim 10^4$ K (~ 10 km s^{-1} for hydrogen). In most models, the clouds are presumed to be organized as part of a general large-scale flow, with small filling factor; however, on velocity scales intermediate between δv and the full velocity width of the line, it is reasonable to suppose that the one-dimensional velocity distributions, comprising clouds drawn from the whole emitting volume, will have essentially uncorrelated velocities, even if, locally, they do have some correlations.

We used Monte Carlo simulations to check how many clouds are needed in order not to create a statistically significant CC($\Delta v = 0$) value. The minimal N_c needed for this is our estimate for the lower limit on the number of clouds NGC 4151. The simulations are very similar to those we used in the case of Mrk 335 (Arav et al. 1997), and better understanding of systematic effects allows us to obtain lower limits up to twice as large as was previously possible for a given simulation. In order to obtain the best lower limit on N_c we simulated the Hα profiles, because the Hα data has the highest S/N. To have the simulation mimic the real CC analysis, we simulated the line segments shown in Fig. 2. These line segments cover only about one third of the total flux in the Hα BEL. Once the lower limit for N_c in this segment is established, we multiply it by a factor of three to obtain the global N_c needed to cover the whole line. It is this number that we present on the CC plots and use in our discussions.

In addition to simulations based on identical clouds we tried cloud distributions. We tested distributions in which $dN_c/dL \propto L^{\alpha}$, where L is the luminosity of the cloud. An example in which $\alpha = -1$ (equal total cloud flux in each luminosity decade) is shown in Fig. 5. The luminosity interval spreads over three decades and the cloud width was chosen to mimic realistic clouds, $b = 50$ km s^{-1}. The top panel shows the CC function in a similar presentation to that in Figs 3 and 4. Although CC($\Delta v = 0$) is not much larger than 1σ, it is evident that a strong CC exists on a velocity scale larger than the size of a single resolution element (6.3 km s^{-1}), because the CC values for the 10 resolution elements around $\Delta v = 0$ are all larger than 1σ. As expected, when we smooth the CC function on the velocity scale of the cloud width, a very significant CC($\Delta v = 0$) emerges (bottom panel). The main reason that the CC($\Delta v = 0$) in this luminosity distribution can be detected, even when $N_c \gtrsim 10^8$ clouds, is that the CC is dominated by the more luminous clouds, because CC $\propto L^2$ and $dN_c/dL \propto L^{-1}$ in this simulation.

In Fig. 6 we show the CC functon for the conservative case of identical clouds. This is the case we use as the firm lower limit for N_c in NGC 4151.

4.2 Flow tubes

Magnetic models (e.g., Rees 1987; Emmering et al. 1992; Bottorff et al. 1997) posit that the emitting as is localized on

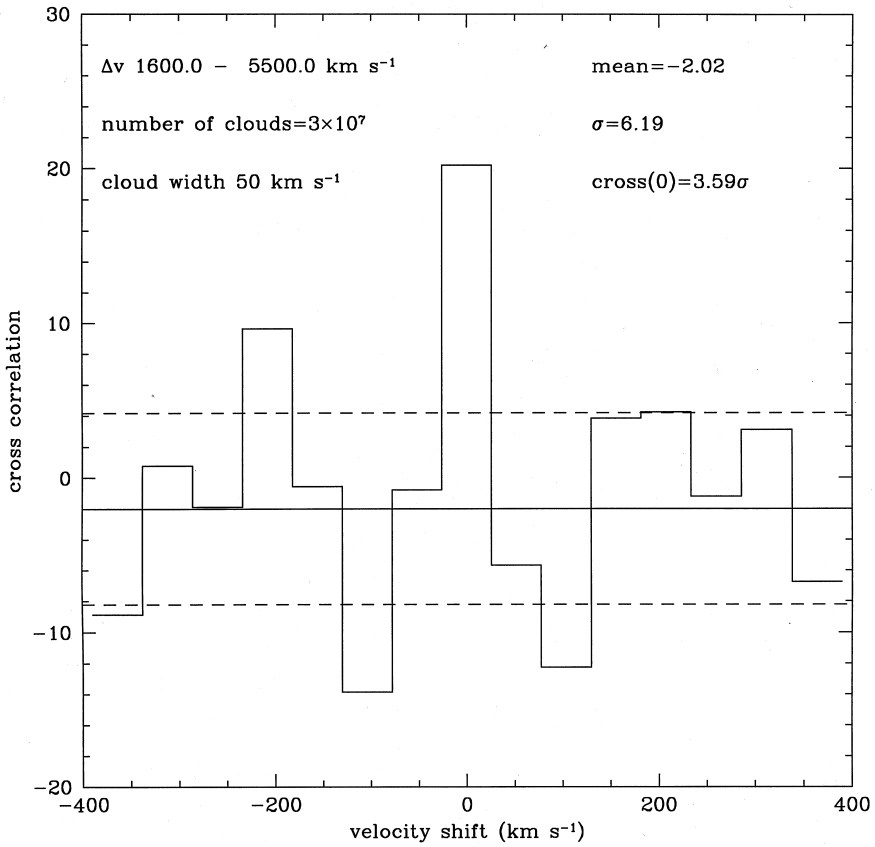

Figure 6. Smoothed CC function for a simulated Hα profile made of 3×10^7 identical clouds, similar to Fig. 5.

individual one-dimensional flux tubes, again with a small volume filling factor. The gas is confined laterally by magnetic stress, but is free to flow along the field lines, satisfying a one-dimensional equation of continuity. The velocity width of the line profile from an individual stream is a significant fraction of Δv, but the full line is formed by the superposition of many such profiles. For geometrically simple flows, like smoothly accelerating radial motion, the full line profiles will naturally be smooth, as we observe. However, more realistic velocity fields, for example as is appropriate when the gas originates from a rotating accretion disc, give sharp edges to line profiles from individual streams, which may be observable.

Let us illustrate this possibility by supposing that the gas flows along a segment of a circle with uniform speed and constant emissivity per unit length. The individual profile will have the form

$$F_v(v) \propto (v_0^2 - v^2)^{1/2}, \qquad v \le v_0. \tag{1}$$

Higher order singularities are possible, but this is the most important and prevalent case. Not all streams contain an extremum in the radial velocity, but, for example, in the solutions computed by Emmering et al. (1992), we estimate that about half of the emission is from gas that will have enough circular motion to make this happen. In actuality this line profile must be convolved with a local velocity-smoothing function that takes account of the thermal width and velocity gradients across a flux tube. Assuming that the individual flux tubes have similar characteristic widths to those derived for the cloud model and that their length is comparable to the size of the BLR, then their number must be smaller than 10^4. In order to interpret our results in this context, we again constructed Monte Carlo simulations. We used flux tubes in the form of quarter circles, where the velocity is constant along the tube (i.e., $v = v_\phi = \text{constant}$), and where the total flux of a given tube is constant. Line profiles were produced in a similar manner to the cloud simulations, with the addition that the positional angles of the flow tubes with respect to the observer were chosen randomly. We also convolved the emission of a single flux tube with a thermal Gaussian ($b = 20$ km s^{-1}). An interesting result of the flux tube simulations is the ease of detection of such structures, even for large velocities. For $v_\phi = 500$ km s^{-1}, 3×10^7 flux tubes gave a clear CC signature, and 10^7 were clearly detected for $v_\phi = 1000$ km s^{-1}. The ease of detection stems from the projected emission profile seen by the observer. Flow tubes can give rise to cusps in the emission profiles, which are very narrow compared with the nominal velocity of the flow. As discussed above, the CC is proportional to the square of the flux at a given velocity position. Thus, relatively few cuspy profiles can dominate the CC function. In addition, a face-on view of the plane of the tube gives rise to emission concentrated in a small Δv, which leads to a similar effect.

4.3 Shock fronts and expanding shells

The next kinematic possibility to consider is a two-dimensional surface, epitomized by a radiative shock forming in the outflow, perhaps enveloping an obstacle or in

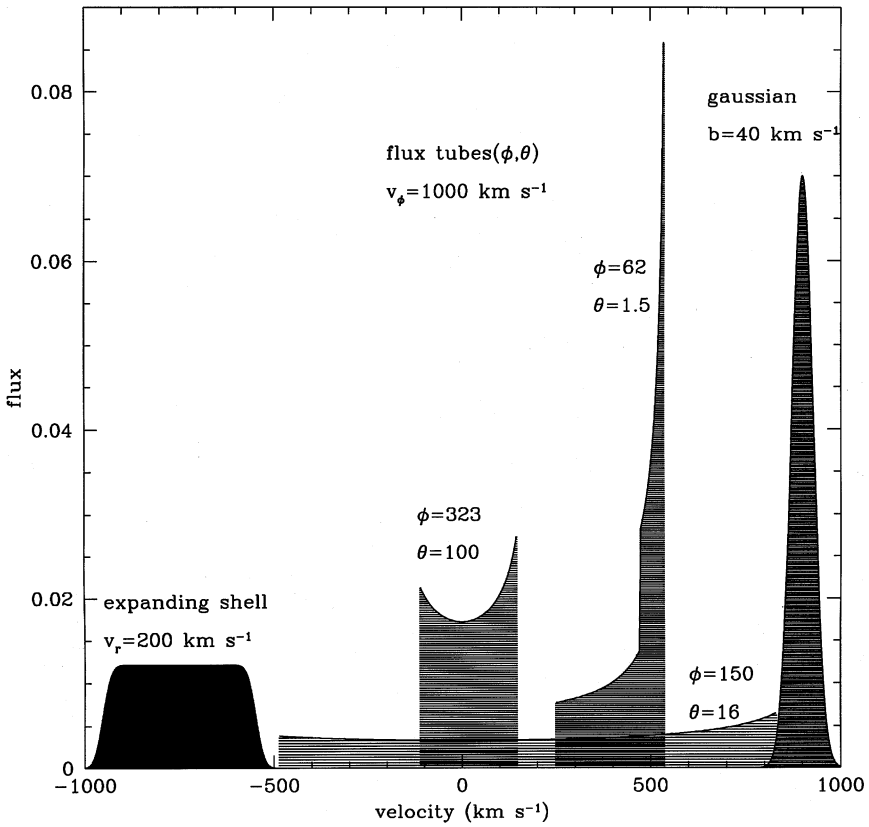

Figure 7. Emission profiles used in the Monte Carlo simulations (see Section 4).

response to variation in the initial flow velocity (Perry & Dyson 1985). Again, we suppose that the emitting gas occupies a small fraction of the volume but that there are a large number of these curved surfaces.

Our elementary model will be a single spherically expanding surface with constant radial velocity v_0 and constant surface emissivity. The observed line profile is given by

$$F_v(v) = \text{const.}, \qquad v \le v_0. \tag{2}$$

We added a pure thermal broadening and found that for shells expanding at 100 km s^{-1} with a thermal broadening of $b = 25$ km s^{-1}, a CC($\Delta v = 0$) is clearly detected for 3×10^6 shells. For similar shells expanding at 200 km s^{-1} the limit is 10^6. The detectability also depends on the gradient of flux as a function of velocity. The smaller the gradient (wider smoothing) at the edges of the profile, the harder it is to detect the CC signature.

In Fig. 7 we show the different emission profiles that we used in the simulations. The three profiles at the centre of the figure are caused by randomly oriented flux tubes with a flow velocity of 1000 km s^{-1} and the same total flux. An edge-on view of the plane of the tubes corresponds to $\theta = 0$, and ϕ is the starting position of the tube, where $\phi = 0$ is along the line of sight. A near face-on view is seen in the $\phi = 323$, $\theta = 100$ case, and a cuspy emission profile is shown in the $\phi = 62$, $\theta = 1.5$ case. A real discontinuity is seen in the cuspy case, which occurs because emission from two different locations along the tube contributes at the same velocity. As the tube is finite, at some point one contribution ends, leading to the discontinuity. In Fig. 7 we did not smooth the emission profile of the flux tube, in order to enhance visually the kinematical effets. In the simulations we smoothed the emission profiles with $b = 20$ km s^{-1}. An expanding shell emission profile and the Gaussian profiles of the clouds (centres shifted to -750 km s^{-1} and 900 km s^{-1}, respectively, for presentation purposes) are also shown in Fig. 7.

4.4 Space-filling flows

Finally, for completeness, we consider flows that are stationary and continuous, filling space over a limited volume in the AGN. A good example is the model of Chiang & Murray (1996). The flow is, by definition, smooth, with a velocity field that must reproduce the observed line profile. No constraint on this model is imposed by our observations.

5 DISCUSSION

Our observational result appears to be in conflict with the simple BEL cloud model, and by extension also with flux tubes and expanding shell models. One possible explanation for the lack of persistent microstructure in the line profiles is that this structure exists but changes on time-scales comparable to or shorter than the time it took to acquire the observations. This possibility is unlikely, because in that amount of time the velocity change for the clouds is too small. The acceleration of the clouds in NGC 4151 can be estimated as follows. From reverberation mapping, Maoz et

al. (1991) estimated the size of the BLR to be 9 light-days, or $R \sim 2 \times 10^{16}$ cm. The velocity of the clouds is given by the width of the BELs ($\sim 5 \times 10^8$ cm s^{-1}). Thus, $a \sim v^2/R \simeq 10$ cm s^{-2}. In the few hours it took to obtain the observations the clouds should therefore accelerate by roughly 1 km s^{-1}. As the CC analysis should be able to detect structure on a scale of ~ 50 km s^{-1} (see Figs 5 and 6), the change in velocity of the clouds caused by acceleration should be negligible.

In addition we note that our underlying assumption in the simulations is that the velocity distribution of the clouds is Poissonian. It is reasonable to expect that if the motion of the clouds is highly ordered on small velocity scales, the resulting CC signature will be easier to detect. It is difficult to imagine a non-contrived way in which an ordered flow could give a smaller CC signature than the Poisson distribution we use. However, if such an ordered distribution existed the limits set by this analysis would be weakened accordingly.

We already showed that the current bloated star models are ruled out by our lower limit on N_c in Mrk 335 (Arav et al. 1997). The NGC 4151 results strengthen this argument considerably, because our lower limit for N_c has risen by an order of magnitude and the expected number of bloated stars is smaller in this less luminous object. Unless the emission width from an individual star is significantly larger than 100 km s^{-1}, the lack of stable microstructure in the line profiles strongly rules out all bloated star models. Even without resorting to the CC analysis, it is easy to demonstrate that for reasonable cloud emission widths, the BELs in NGC 4151 cannot be made from 10^4–10^5 individual emitters, which is the maximum allowed number of bloated stars. Fig. 8 shows part of the Hα data from the combined exposures, and three simulations of the same segment. We have used the same noise but different cloud distributions in each simulation. The amount of structure in the simulations, as contrasted with the smoothness of the data, shows that either the observed Hα profile is made from many more than 3×10^5 clouds or the emission width of an individual cloud is much larger than $b = 80$ km s^{-1}. The structure that is seen in the data is on scales of 500–1000 km s^{-1} and is difficult to associate with individual units of sonically connected material, but can be associated with a smooth flow or disc models. To the eye it also seems that the data has structure on scales of ~ 50 km s^{-1}, but the CC analysis have shown that this structure does not repeat in two different observations.

From the Monte Carlo simulations, it is clear that strong constraints can also be applied to emission models that do not arise from point-like structures (i.e. clouds). For example, although we only used one simple choice of flow tube, some general conclusions can be deduced from the simulations of this case. It appears that the number of ran-

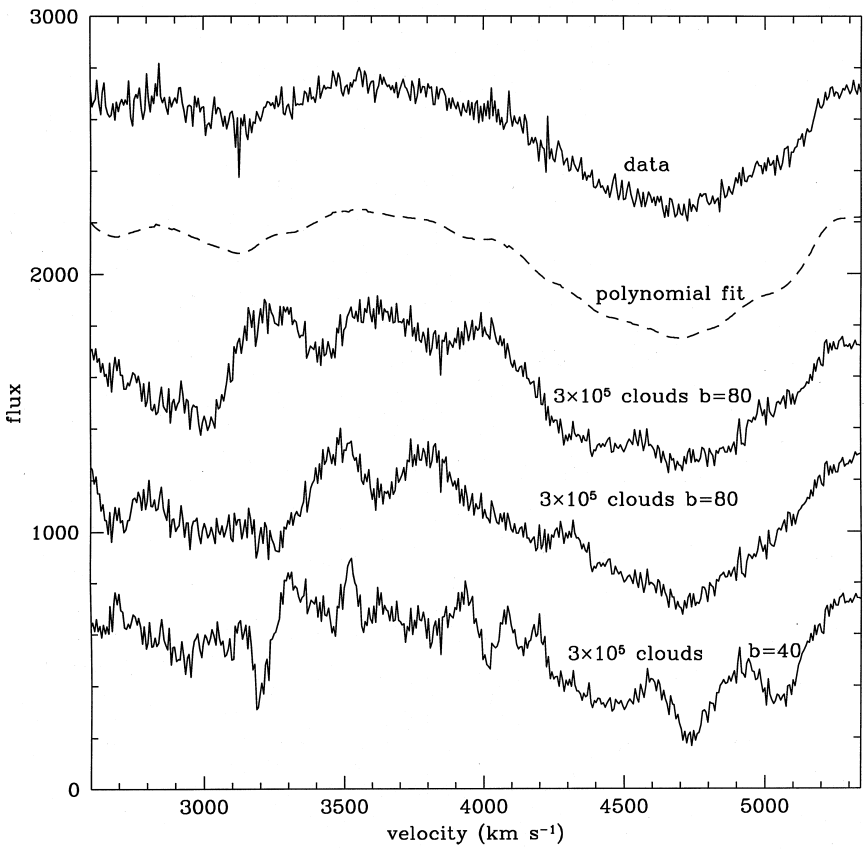

Figure 8. A qualitative comparison between the observed Hα line (top curve) and simulated ones (bottom three curves) shows how difficult it is to create a smooth enough profile from 3×10^5 clouds even for very broad individual cloud emission. All the curves are shown on the same scale, which is five times magnified in the y axis and 1.42 times magnified in the x direction with respect to the Hα segment shown in Fig. 2. A linear function was subtracted from the profiles in order to obtain a flat presentation. The dashed curve shows the polynomial fit for the data that were used in creating the simulated profiles.

domly oriented flow tubes must be very large in order to conceal a significant CC($\Delta v = 0$). This result holds even for flux tubes that, on average, span a significant fraction of the velocity width of the line. In order for a flow-tube emission model not to produce a CC signature, one or more of the following constraints must hold.

(i) The number of flow tubes is very large.
(ii) Emission cusps in projected velocity are somehow avoided.
(iii) The flow tubes are organized in a way that mimics a smooth, ordered flow.
(iv) The velocity width perpendicular to the axis of the tube is substantial ($\gtrsim$100 km s^{-1}) and thus dampens the effect of the narrow emission cusps.

As noted in Section 1, photoionization arguments give the highest model-independent (i.e. irrespective of the microphysics of the clouds) estimate for N_c. In NGC 4151, these arguments lead to an upper limit estimate of 10^6–10^7 clouds (extrapolated from Arav et al. 1997, but see caveats therein and in Section 1). This upper limit is smaller by about an order of magnitude than the one in Mrk 335 because of the lower luminosity of NGC 4151 or, more precisely, its smaller BLR size. In contrast, our lower limit for N_c in this object has increased by an order of magnitude to 3×10^7–10^8. While the Mrk 335 result does not put a strong constraint on the generic cloud picture, our current result does. The photoionization estimates can be pushed up, but at the price of becoming more contrived. The constraint our results puts on any cloud picture is strong enough to suggest that the BELs do not originate from discrete quasi-static structures, and this strengthens the case for emission models that create the BELs from a continuous flow or in an accretion disc.

ACKNOWLEDGMENTS

We thank S. Vogt for leading the construction of the HIRES spectrograph and Michael Rauch for assisting with the observations. NA and RDB acknowledge support from NSF grants 92-23370 and 95-29170. AL acknowledges support from the E. and J. Bishop research fund, and from the Milton and Lillian Edwards academic lectureship fund.

REFERENCES

Alexander T., Netzer H., 1994, MNRAS, 270, 803
Arav N., Barlow T., Laor A., Blandford R. D., 1997, MNRAS, 288, 1015
Atwood B., Baldwin J. A., Carswell R. F., 1982, ApJ, 257, 559
Barlow T., Sargent W. L. W., 1997, AJ, 113, 136
Bottorff M., Korista K. T., Shlosman I., Blandford R. D., 1997, ApJ, 479, 200
Chiang J., Murray N., 1996, ApJ, 466, 704
Crenshaw D. M. et al., 1996, ApJ, 470, 322
Edelson R. A. et al., 1996, ApJ, 470, 364
Emmering R. T., Blandford R. D., Shlosman I., 1992, ApJ, 385, 460
Ferland G. J., Rees M. J., 1988, ApJ, 332, 141
Kaspi S. et al., 1996, ApJ, 470, 336
Kazanas D., 1989, ApJ, 347, 74
Krolik J. H., McKee C. F., Tarter C. B., 1981, ApJ, 249, 422
Maoz D. et al., 1991, ApJ, 367, 493
Netzer H., 1990, in Blandford R. D., Netzer H., Woltjer L., eds, Saas-Fee Advanced Course 20: Active Galactic Nuclei. Springer, New York, p. 57
Perry J. J., Dyson J. E., 1985, MNRAS, 213, 665
Rees M. J., 1987, MNRAS, 228, 47P
Scoville N., Norman C., 1989, ApJ, 332, 162